Spectrochimica Acta, Vol. 49A, No. 12, pp. 1735–1749, 1993
Printed in Great Britain

0584-8539/93 $6.00 + 0.00

Normal coordinate analysis of bilirubin vibrational spectra: effects of intramolecular hydrogen bonding

BIJUN YANG, ROBERT C. TAYLOR and MICHAEL D. MORRIS
Department of Chemistry, University of Michigan, Ann Arbor, MI 48109, U.S.A.

and

XIU-ZHEN WANG, JIN-GUANG WU, BAO-ZHU YU and GUANG-XIAN XU
Department of Chemistry, Peking University, Beijing, 100871, China

and

ROGER D. SOLOWAY
Division of Gastroenterology, University of Texas Medical Branch, Galveston TX 77550, U.S.A.

(*Received* 19 *September* 1992; *accepted* 24 *January* 1993)

Abstract—Normal coordinate analyses are presented for half-bilirubin molecules. Calculations for the A–B pyrromethenone include intramolecular hydrogen bonds, while those for the C–D chromophore exclude intramolecular hydrogen bonds. Valence force-field parameters have been optimized to correlate closely with the IR and Raman spectra of the target molecules. The results of the calculations are compared with the spectra of bilirubin IXa and various model compounds in the solid state and solution.

INTRODUCTION

VIBRATIONAL spectroscopy is emerging as an important tool in the study of the structure of bilirubin in physiological and model matrices related to its role in liver pathology and in neonatal jaundice. Infrared microspectroscopy is increasingly used to examine the local structure of bilirubin in gallstones [1–3], both as a clinical diagnostic and as a probe of the mechanism of gallstone formation. Resonance Raman microspectroscopy has also been proposed as a diagnostic for bilirubin gallstones [4, 5]. Resonance Raman spectroscopy has been used to study changes in intramolecular hydrogen bonding in the bilirubin–albumin complex [6] and in bilirubin phospholipid complexes [7]. Even surface-enhanced Raman spectroscopy has been applied to the bilirubin–albumin complex system [8].

Bilirubin vibrational Raman spectroscopy has been impeded by lack of rigorous band assignments for the molecule. Early workers largely used group frequency correlations [9] from the standard IR spectroscopy literature. The Warshel–Daub procedure has been used to assign some of the bands of the bilirubin resonance Raman spectrum [10], but the agreement with experiment was not completely satisfactory and required the *ad hoc* assumption that the exo vinylpyrromethenone has a higher energy electronic transition than the endo vinylpyrromethenone in the acid form and that the order was reversed in the dianion. One of our laboratories has previously reported calculations for several bands in the aromatic ring mode and carbonyl stretching regions and have verified these with IR spectroscopy of the normal and deuterated bilirubins [11]. We have reported empirical assignments, largely correlations with the pyrrole or lactam moieties of the exo and endo vinylpyrromethenones, based on studies of an extensive series of model compounds [6, 7]. Considerable disagreement exists amongst these studies as to the band assignments and calculated frequencies.

In the present study we present normal coordinate calculations of the vibrational modes of both structures of bilirubin, using a valence force field. We place special emphasis on the aromatic ring mode region and carbonyl stretching region (*ca*

900–1700 cm^{-1}). These regions dominate the resonance Raman spectra and have been emphasized in most IR experiments as well. Calculations including and excluding the effects of intramolecular hydrogen bonds have been performed. We present new data on the spectra of deuterated bilirubins, as well as on new model compounds with perturbed propionic acid side chains.

It has long been appreciated that the solution chemistry of bilirubin is influenced by intramolecular hydrogen bonding. Similarly intramolecular hydrogen bonding should be an important aspect of the structures of the mixed bilirubin salts which are in bilirubin gallstones. Thus, both the solution and the solid phase hydrogen bonding are physiologically important.

EXPERIMENTAL

Mid-IR spectra of bilirubin (Sigma, reagent grade) were measured (Nicolet 7199B FTIR) at 2 cm^{-1} resolution in KBr pellets, fluorolube mulls and by photoacoustic spectroscopy of the pure solid. Far-IR (20–200 cm^{-1}) spectra were measured at 4 cm^{-1} resolution using mineral oil or petroleum jelly mulls in polyethylene cells. Resonance Raman spectra of solid bilirubin were measured at 5 cm^{-1} resolution in KBr pellets using a double monochromator (Spex 1401), photon counting and argon in 488 or 514.5 nm excitation. FT-Raman spectra were taken with a Nicolet 910 spectrometer at 4 cm^{-1} resolution.

Deuterated bilirubin was prepared by replacement of the six labile protons by dissolution of solid bilirubin in 0.001 M $NaOH/D_2O$ followed by reacidification in 1 M DCl/D_2O. The deuterated solid was washed several times with D_2O and $CDCl_3$ and desiccated in a nitrogen atmosphere to remove residual solvent. Spectra of the perdeuterated compound were taken as fluorolube mulls.

The model compounds α, α'-dimethylmesobilirubin (MBR) in the meso and racemic forms were prepared as described previously [12]. Resonance Raman spectra were obtained at a concentraion of 5×10^{-4} M in chloroform solvent. The resonance Raman spectra of these compounds were measured with Nd–YAG second harmonic (532 nm) excitation with a triple spectrograph/array detector instrument at 1 cm^{-1} resolution.

NORMAL COORDINATE ANALYSES

Structure

Bilirubin IXa (structure 1) has two pyrromethenone rings (A–B or endo and C–D or exo) that lie in two planes 97° apart. It contains 82 atoms in all. In the electronic ground state, there is no conjugation between the two rings. For simplicity, we use a model containing 44 atoms, which is just slightly larger than the A–B ring. However, we have calculated all of the modes of the A–B system, including the effect of the hydrogen bond, modeling them as shown in Fig. 1. The vibrational modes of this model will be the modes of a complete bilirubin molecule or the model compounds possessing the intramolecular hydrogen-bonded structure. Additionally, we have calculated the modes in the aromatic ring stretch and carbonyl ring stretching regions for the C–D rings, omitting the hydrogen bonds. In the latter calculations, we also modeled the methyl and propionic side groups as their carbon atoms for simplicity. We used this simplified model to describe the bilirubins lacking intramolecular hydrogen bonds. This structure is observed in the bilirubin/sphingomyelin complex and in bilirubin/calcium salts [1–7]. The predictions can be tested against the published Raman spectra of vinylisoneoxanthobilirubinate, which has an exo-vinyl group.

The bond lengths and angles of bilirubin used to calculate Cartesian coordinates of pyrromethenone are from X-ray studies [13]. Diagrams of the molecules plotted in these Cartesian coordinates are shown in Figs 1 and 2. Force constants are taken from 2-pyrrolidinone, pyrroles, lactams and related compounds [14–17]. For hydrogen bond stretching, a force constant of 0.05 mdyn $Å^{-1}$, which is typical [18], was used. For hydrogen bond bending 0.005 mdyn $Å^{-1}$ was used.

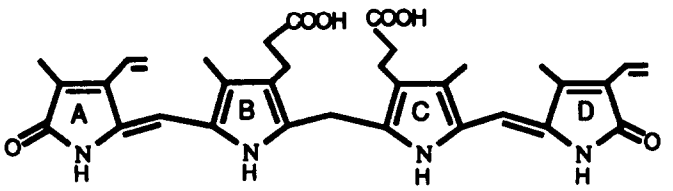

Structure 1

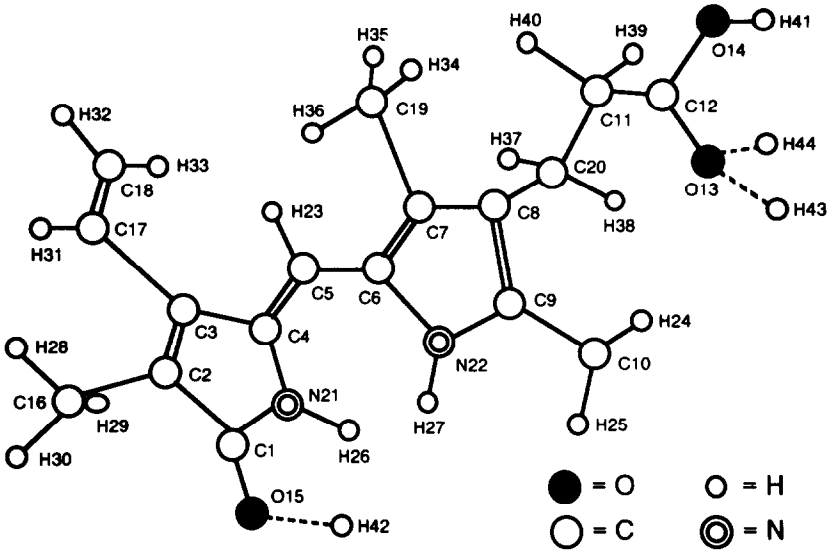

Fig. 1. Two-dimensional model of bilirubin IXα (A–B) pyrromethenone.

Method

The general methods of normal coordinate analysis have been described in detail [19, 20]. The programs used in this work were written at the University of Michigan (C–D rings, interaction force constants, no hydrogen bonding) and Beijing University (A–B ring, hydrogen bonding) and are derived from classical public domain F–G matrix programs [21, 22]. If we include the protons on the methyl and propionic acid side chains, there are 132 internal coordinates and 126 normal vibrations. Excluding these protons leaves 82 internal coordinates and 60 normal vibrations.

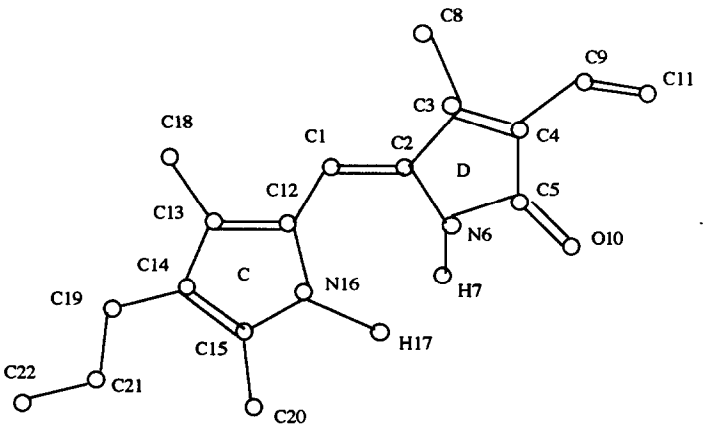

Fig. 2. Two-dimensional model of bilirubin IXα (C–D) pyrromethenone.

Table 1. Internal coordinates and optimized force constants of bilirubin (AB) pyrromethenone

No.	Internal coordinates	Vibration mode	Force constant
	Stretch		*mdyn Å*$^{-1}$
1.	*Q*1	C–O (–H)	8.12
2.	*Q*2, *Q*3	C–O	8.4
3.	*Q*4	N–C (lactam)	7.0
4.	*Q*5, *Q*6, *Q*7	N–C	3.0
5.	*Q*8, *Q*9, *Q*10	C=C (ring)	7.6
6.	*Q*11–*Q*21	C–C	3.3
7.	*Q*22, *Q*23	C=C (bridge)	6.8
8.	*Q*24–*Q*29	C–H (–CH_3)	4.67
9.	*Q*30, *Q*31	C–H (C=CH_2)	5.0
10.	*Q*32–*Q*37	C–H (–CH_2)	4.76
11.	*Q*38, *Q*39	C–H (–CH=)	5.1
12.	*Q*40	N–H (lactam)	5.82
13.	*Q*41	N–H (pyrrole)	6.37
14.	*Q*42, *Q*44, *Q*45	O···H (H bonding)	0.05
15.	*Q*43	O–H	3.97
	Bend		*mdyn Å rad*$^{-2}$
16.	*Q*46–*Q*49, *Q*62–*Q*62, *Q*66–*Q*69	(∠CCC (C=C)	0.7
17.	*Q*50–*Q*53, *Q*65	∠CCN	0.5
18.	*Q*54, *Q*55	∠CNC	0.75
19.	*Q*56, *Q*65	∠OCN	0.5
20.	*Q*57–*Q*59	∠CCC	0.5
21.	*Q*60, *Q*61	∠HNC	0.41
22.	*Q*70, *Q*71	∠CCO	0.5
23.	*Q*72	∠OCO	0.5
24.	*Q*73–*Q*78	∠CCH (–CH_3)	0.37
25.	*Q*79–*Q*82, *Q*85, *Q*88	∠HCH	0.50
26.	*Q*83, *Q*84	∠CCH (vinyl –CH_2)	0.45
27.	*Q*86, *Q*87	∠CCH (bridge)	0.50
28.	*Q*89–*Q*96	∠CCH (vinyle)	0.49
29.	*Q*97–*Q*100	∠CCH (bridge)	0.59
30.	*Q*101–*Q*104	∠COH	0.552
31.	*Q*105	∠CO···H	0.005
	Torsion		
32.	*Q*106–*Q*124	Groups connected with lactam or pyrrole, or on the rings, e.g. $C_5C_4N_{21}C_1$	0.24
	Wagging		
33.	*Q*125–*Q*132	Out-of-plane vibrations, e.g. O_{15}–$C_1C_2N_{21}$	0.11

Table 1 lists the internal coordinates and optimized force constants used in the detailed A–B calculations. Table 2 lists the internal coordinates and force constants used in the C–D ring calculations.

Results and Discussion

Table 3 lists the calculated and observed frequencies for the A–B pyrromethenone obtained from the detailed calculations, as well as experimental IR and Raman frequencies obtained for solid bilirubin. Table 4 lists aromatic ring and carbonyl frequencies for the C–D pyrromethenone obtained from the simplified model and the corresponding experimental values from vinylisoneoxanthobilirubinate. Selected IR frequencies of the perdeuterated compound are listed in Table 5.

The bands in the low frequency region are wagging, torsion and bending modes of bilirubin. We present them for the A–B ring system only. The agreement between calculated and measured frequencies is good in this region.

Table 2. Internal coordinates and valence force constants of bilirubin (C–D) pyrromethenone

No.	Internal coordinates	Major force constants Vibration mode	Force constant
	Stretch		*mdyn Å*$^{-1}$
1.	*Q*1	C=C (bridge)	8.212
2.	*Q*2, *Q*4	C–C (lactam)	4.174
3.	*Q*3	C=C (lactam)	8.653
4.	*Q*5	N–C (=O)	5.623
5.	*Q*6, *Q*16, *Q*80	C–N (=C)	7.695
6.	*Q*7, *Q*8, *Q*18, *Q*19	C–C* (β)	4.743
7.	*Q*9	C=O	11.795
8.	*Q*10	N–H (lactam)	6.711
9.	*Q*11, *Q*13, *Q*15	C=C (vinyl, pyrrole)	8.366
10.	*Q*12, *Q*20	C–C* (α)	4.756
11.	*Q*14	C–C (pyrrole)	5.999
12.	*Q*17	N–H (pyrrole)	6.864
13.	*Q*21, *Q*22	C–C (propionic)	4.802
	Bend		*mdyn Å rad*$^{-2}$
14.	*Q*23, *Q*40, *Q*51	∠CCC* (α)	0.620
15.	*Q*24, *Q*41, *Q*52	∠NCC*	0.620
16.	*Q*25, *Q*28, *Q*42, *Q*45	∠CCN (ring)	1.277
17.	*Q*26, *Q*27, *Q*43, *Q*44	∠CCC	1.277
18.	*Q*29, *Q*46	∠CNC	1.671
19.	*Q*30–*Q*33, *Q*47–*Q*50	∠CCC* (β)	0.595
20.	*Q*34	∠OCC	0.945
21.	*Q*35	∠OCN	0.945
22.	*Q*36, *Q*37	∠HNC (lactam)	0.411
23.	*Q*38, *Q*39	∠CCC (vinyle, bridge)	0.795
24.	*Q*53, *Q*54	∠HNC (pyrrole)	0.438
25.	*Q*55, *Q*56	∠CCC (propionic)	1.032
	Wagging		
26.	*Q*57, *Q*61, *Q*64	C* (α)–CCN	0.409
27.	*Q*58, *Q*59, *Q*62, *Q*63	C* (β)–CCC	0.509
28.	*Q*60	O–CCN	0.686
29.	*Q*65	H–NCC (pyrrole)	0.121
30.	*Q*66	N–NCC (lactam)	0.140
31.	*Q*67	C–CCC (vinyle)	0.509
32.	*Q*68, *Q*69	C–CCC (propionic)	0.500
	Torsion		
33.	*Q*70–*Q*79	Groups connected with lactam or pyrrole, or on the rings, e.g. N_6C_2–C_3C_4	1.270
34.	*Q*81	N_6C_2–C_1C_{12}	0.579
35.	*Q*82	$N_{16}C_{12}$–C_1C_2	0.041
		Interaction force constants	
	Stretch–stretch (*pyrrole ring*)		
36.		C=C, C–C C=C, C–N; C common	0.764
37.		C=C, C=C	−0.764
38.		C–C, C–N	−0.791
39.		C=C, C–N; C not common	−0.349
	Stretch–stretch (*lactam ring*)		
40.		C–C, C=C	0.256
41.		C–C, C–C	0.155
42.		C–C, C–N; C not common	−0.065

continued on next page

Table 2. *continued*

No.	Internal coordinates	Major force constants Vibration mode	Force constant
43.		C–C, C–N; C common	0.421
44.		C–C, C=O; C not common	−0.124
45.		C–C, C=O; C common	0.576
46.		C=C, N–C	0.059
47.		C=O, N–H	−0.009
48.		C–N, C=O; C common	1.114
49.		C–N, C=O; C not common	−0.216
50.		C–N, N–H	0.036
	Stretch–stretch		
51.		C–N, C–N	0.943
52.		C–N, C–C* (*a*); C common C–C, C–C* (*b*); C common	0.053
53.		C=C, C–C* (*a*); C common C=C, C–C* (*b*); C common	0.053
54.		C†–C*, C*–C; C* common C‡–C†, C†–C*; C† common	0.083
	Stretch–bend		
55.		C–N, ∠N–C–C*; C–N common C–N, ∠C–N–H; C–N common C=C, ∠C=C–C* (*a*); C=C common C=C, ∠C=C–C* (*b*); C=C common C–C, ∠C–C–C*	0.119
56.		C–N, ∠C=C–C* (*a*); C common C–N, ∠C–N–H; N common C=C, ∠N–C–C*; C common C=C, ∠C–C–C*; C common C–C, ∠C=C–C* (*b*)	−0.119
57.		C–C, ∠C–C=C C–N, ∠N–C=C; C–N common C=C, ∠N–C=C; C=C common C=C, ∠C–C=C; C=C common C–N, ∠C–N–C	1.127
58.		C–C* (*a*), ∠N–C–C* C–C* common C–C* (*a*), ∠C=C–C* (*a*); C–C* common C–C* (*b*), ∠C=C–C* (*b*); C–C* common C–C* (*b*), ∠C–C–C*; C–C* common	0.617
59.		C=O, ∠O=C–N C=O, ∠O=C–C	0.047
60.		C=O, ∠H–N–C	0.025
61.		N–H, ∠O=C–C N–H, ∠O=C–N	−0.024
	Bend–bend		
62.		∠C–C–C*, ∠C–C–C*	0.016
63.		∠C=C–C* (*a*), ∠C=C–C* (*b*); C=C common ∠N–C–C*, ∠C–N–H; C–N common	
64.		∠C–N–C, ∠N–C–C* ∠N–C=C, ∠C=C–C* (*b*); C=C common ∠C–C=C, ∠C=C–C* (*a*); C=C common ∠N–C=C, ∠C–N–H, C–N common	0.084
	Wagging–wagging		
65.		C–C* (*a*), C–C* (*a'*)	0.027
66.		C–C* (*b*), C–C* (*b'*)	−0.030
67.		C–C* (*a*), C–C* (*b*)	−0.053
68.		C–C* (*a*), C–C* (*b'*)	0.020
69.		O=C, H–N	−0.039

continued on next page

Table 2. *continued*

No.	Internal coordinates	Major force constants Vibration mode	Force constant
		Wagging–torsion	
70.		C–C* (*a*), *t*(*ab*)	0.314
71.		C–C* (*b*), *t*(*ab*)	−0.296
72.		C–C* (*a*), *t*(*a'b'*)	−0.068
73.		C–C* (*b*), *t*(*a'b'*)	−0.090
		Torsion–torsion	
74.		*t*(*ab*), *t*(*a'b'*)	−0.229

* Methyl carbon attached directly to rings.
† One carbon away from C*.
‡ Two carbons away from C*.

In the 900–1700 cm^{-1} region many modes are strongly resonance enhanced. This region has been emphasized in resonance Raman studies and has several strong and empirically useful IR bands as well. We discuss each of the bands in detail.

The hydrogen-bonded A–B calculation places a 965 cm^{-1} vibration on the pyrrole ring. It is the stretching of the methyl carbon connected to the pyrrole, and a stretching of C(9)–N(22). The non-hydrogen bonded C–D model predicts a mode at 945 cm^{-1}, which describes a stretch extending to the lactam moiety. In solution, this mode has previously been observed to be strongly hydrogen bond dependent [6, 7]. Thus, the extended assignment conforms more closely to the environmental sensitivity.

The A–B model calculation localizes 995 cm^{-1} as a lactam vinyl group bending. In the resonance Raman spectrum there is a strong band at 997 cm^{-1} in bilirubin XIIIα (A–B rings only). This band is relatively stable to the hydrogen bonding changes and shifts about 10 cm^{-1} in MBR XIIIα, in which the vinyl groups are replaced by ethyl groups. The assignment is realistic. There is, in addition, a propionic acid side C–O–H bending mode predicted at 982 cm^{-1}. This would be observed in the IR but would not be seen in the resonance Raman spectra.

The non-hydrogen-bonded model predicts a torsion of the exo C=C group connecting the lactam and pyrrole moieties and bending of the vinyl group at 1032 cm^{-1} for the C–D ring. The band at about 1032 cm^{-1} is weak in vinylisoneoxanthobilirubinate.

In both sets of calculations the band in the 1060 cm^{-1} region is assigned largely to a pyrrole ring stretching mode. In the resonance Raman spectra of all model compounds reported, including the monomeric forms, there is a medium or strong hydrogen bond insensitive band in the 1050–1060 cm^{-1} region, confirming the pyrrole assignment.

The more detailed A–B model finds propionic acid methylene bending C–H bending modes at 1087 and 1106 cm^{-1}, which agree well with the 1092 and 1107 cm^{-1} bands observed in the bilirubin IR and Raman spectrum.

The non-hydrogen-bonded model also predicts a C–D vinyl C=C, exo C=C and lactam, pyrrole C–N stretch at 1107 cm^{-1}. This band is not well resolved from the strong and broad 1056 cm^{-1} band in the monomeric compounds but is a medium-to-strong peak in the spectra of bilirubin IIIα, XIIIα and IXα. The mode composition may be fairly realistic, because it shifts about 5 cm^{-1} or more from bilirubin IIIα (bilirubin XIIIα) to meso bilirubin XIIIα where the vinyl group is replaced by an ethyl group. This strong vinyl group sensitivity confirms our assignment.

The simplified model calculates a pyrrole in-plane methyl deformation at 1144 cm^{-1} in the C–D system. We equate this band with the band observed in the Raman spectrum at 1141 cm^{-1} in vinylisoneoxanthobilirubinate aqueous solution. This assignment may be a good one since this band appears to have a big shift or be a new band peculiar to the half bilirubin molecule. The significant changes in the spectra, in this case, should affect the pyrrole ring more than that of the lactam ring.

The A–B model predicts a vinyl ethylenic stretching and bending mode of the lactam at 1173 cm^{-1}, which is equated to the 1164 cm^{-1} band in the IR (1180 cm^{-1}, weak, in the

Table 3. Calculated and observed frequencies and potential energy distribution PED

Calcd	Raman RR	Raman FT-R	IR	Assignment and PED (%)
3409			3410	N_{22}–H_{27} 1.0
3260			3262	N_{21}–H_{26} 1.0
3101		3097	3101	C_{18}–H_{33} .49, Cl_8H_{32} .48
3071		3070	3070	C_5–H_{23} .99
3002		3007	3011	C_{20}–H_{38} .31, C_{20}–H_{37} .29, C_{11}–H_{40} .21, C_{11}–H_{39} .19
2968		2965	2968	C_{19}–H_{36} .69, C_{19}–H_{35} .17, C_{19}–H_{34} .13
2924		2918	2913	C_{10}–H_{24} .49, C_{10}–H_{25} .50
2857		2852	2858	C_{19}–H_{34} .35, C_{19}–H_{35} .35, C_{19}–H_{36} .31
2680			2673	O_{14}–H_{41} 1.0
1688	1680		1692	C_{12}–O_{14}, .42 C_{12}–O_{13} .47
1655	1637	1650	1649	C_1–O_{15} .36, N_{21}–C_1 .17, C_3–C_2 .13
1606	1614	1610	1612	C_3–C_2 .26, C_1–O_{15} .15, C_6–C_7 .13, N_{21}–C_1 .10
1567	1569	1570	1571	C_6–C_7 .30, C_4–C_5 .21, C_3–C_2 .09
1487	1504	1502	1500	$H_{32}C_{18}H_{33}$ .22, $H_{31}C_{17}C_{18}$ .21, $H_{31}C_{17}C_3$ .17
1448	1456	1451	1441	C_{11}–C_{12} .27, C_{12}–O_{13} .22, C_{12}–O_{14} .23
1395	1395	1404	1405	N_{21}–C_1 .17, $H_{28}C_{16}H_{30}$ .11, C_1–C_2 .13
1356	1365	1363	1364	$H_{28}C_{16}H_{30}$ .12, $H_{35}C_{19}H_{36}$ .11, $H_{34}C_{19}H_{36}$ .11
1353	1340	1340	1344	$H_{35}C_{19}H_{36}$ .11, $H_{34}C_{19}H_{36}$ .10
1310	1291	1290	1301	$H_{23}C_5C_4$ .24, C_4–C_5 .20, N_{21}–C_1 .15, $H_{23}C_5C_6$ .16
1243	1248	1245	1250	$C_{20}C_{11}H_{39}$ .14, $H_{39}C_{11}C_{12}$ .10, C_7–C_8 .10
1225			1220	C_3–C_4 .19, C_3–C_{17} .16, $H_{31}C_{17}C_3$ .09
1187	1190	1191	1186	N_{22}–C_9 .13, C_7–C_8 .11, N_{22}–C_6 .08
1173	1168	1160	1164	C_{17}–C_{18} .41, $H_{31}C_{17}C_{18}$ .12, $C_{17}C_{18}H_{33}$ .09
1106			1107	$C_{11}C_{12}H_{37}$ .17, $C_8C_{20}H_{37}$ .16, $C_{11}C_{20}H_{38}$ .14, $C_8C_{20}H_{38}$ .12, $C_{20}C_{11}H_{39}$ .10
1087	1096	1088		$H_{40}C_{11}C_{12}$ .19, $C_{20}C_{11}H_{40}$ .18, $H_{39}C_{11}C_{12}$ .14, $C_{20}C_{11}H_{39}$ .12
1057	1048	1060	1050	C_9–C_{10} .17, N_{22}–C_9 .15, C_5–C_6 .10, C_7–C_8 .10
1015		1009		N_{21}–C_4 .15, C_2–C_{16} .15, N_{22}–C_6 .08, $H_{26}N_{21}C_1$ .11, C_1–O_{15} .10
995	988	992	994	$C_{17}C_{18}H_{32}$ .29, $C_{17}C_{18}H_{33}$ .27
982			983	$C_{12}O_{14}H_{41}$ .88
965	948	950	935	C_8–C_{20} .17, $C_9C_{10}H_{24}$ .16, C_7–C_{19} .12, N_{22}–C_9 .09
905		900		$C_9C_{10}H_{24}$ .23, $C_9C_{10}H_{25}$ .18
835	845	835	844	$C_2C_{16}H_{30}$ .29, $C_2C_{16}H_{28}$ .23
826	825		820	$C_7C_{19}H_{34}$ .15
796		790	790	$H_{27}N_{22}C_6$ .11 $C_2C_{16}H_{29}$ .24
729	725	738		$C_7C_{19}H_{34}$ .08
700	700		698	H_{26}–$N_{21}C_1C_4$ .42, $C_3C_5C_4$–$N_{21}H_{26}C_1$ .25, $O_{15}C_2C_1$–$N_{21}C_4H_{26}$ .23
665			669	H_{23}–$C_5C_4C_6$ .11
643		638		$C_{12}O_{13}H_{43}$ .53, $N_{21}C_3C_4$–$C_5H_{23}C_6$ .19, $C_4H_{23}C_5$–$C_6C_7N_{22}$ .11
629			626	$C_3H_{31}C_{17}$–$C_{18}H_{32}H_{33}$ .82, $C_4C_2C_3$–$C_{17}H_{31}C_{18}$ .16
6611	610	610	601	N_{21}–C_4 .12, $C_4C_5C_6$ .11
576	585	580		$C_2N_{21}C_1$–$O_{15}H_{42}$ .85
548	555	560	555	$C_8C_{20}H_{38}$ .24, $C_{11}C_{20}H_{38}$ .25, $C_{11}C_{20}H_{37}$ .18, $C_8C_{20}H_{37}$ .14
498	508	495	491	$C_2C_{16}H_{30}$ .16, $C_3C_{17}C_{18}$ .13, $C_2C_{16}H_{28}$ .11
473		470	478	$N_{22}C_8C_9$–$C_{10}H_{24}H_{25}$ .69
458			457	$C_1N_{21}C_4$ .13, $N_{22}C_8C_9$–$C_{10}H_{24}H_{25}$ .11
438		430	432	$N_{22}C_8C_9$–$C_{10}H_{24}H_{25}$ .12, $C_8C_{20}C_{11}$ .16, $C_{20}C_{11}C_{12}$ .16, $C_{11}O_{14}C_{12}$–$O_{10}H_{24}H_{25}$ .13
417		415	416	$C_1C_3C_2$–$C_{16}H_{28}H_{29}H_{30}$ .37
394	392	390		$C_6C_8C_7$–$C_{19}H_{34}H_{35}H_{36}$ .23
384	378	385	383	$C_6C_8C_7$–$C_{19}H_{34}H_{35}H_{36}$ .45, $O_{14}C_{11}C_{12}$–$O_{13}H_{43}H_{44}$ .11
344				O_{15}–$C_1N_{21}C_2$ .33, C_{16}–$C_2C_1C_3$ .25, $C_1C_3C_2$–$C_{16}H_{28}H_{29}H_{30}$ .11
336		330		$H_{23}C_4C_5$–$C_6C_7N_{22}$ .14
303		300	302	O_{15}–H_{42} .62

continued on next page

Table 3. *continued*

Calcd	Raman RR	Raman FT-R	IR	Assignment and PED (%)
298	298			O_{13}–H_{44} .74
289	282	280	282	O_{13}–H_{43} .59, O_{13}–H_{44} .10
265	265	250	248	$C_3C_4C_2$–$C_{17}H_{31}C_{18}$ .16, O_{15}–$C_1N_{21}C_2$ .24, C_{17}–$C_3C_2C_4$ .14
236	226			C_{19}–$C_7C_6C_8$ .23, $H_{37}H_{38}C_8C_{20}$–$C_{11}C_{12}H_{39}H_{40}$ .10
217			226	C_{20}–$C_8C_9C_7$ .15, $C_7C_9C_8$–$C_{20}C_{11}H_{37}H_{38}$ .16
199	195	200	202	$O_{15}C_1N_{21}$ .15, C_5–C_6 .10
193	192		187	$O_{15}C_2C_1$–$N_{21}C_4H_{26}$ .15, $C_1C_{16}C_2$–$C_3C_{17}C_4$ .13, C_{17}–$C_3C_2C_4$ .10
167	170		171	$C_{19}C_7C_8$ .23, $C_{10}C_9N_{22}$ .29
156	160		152	$C_6C_{19}C_7$–$C_8C_{20}C_9$ .17, $C_5C_7C_6$–$N_{22}C_9H_{27}$ .13
147		145	145	$C_{10}C_9C_8$–$N_{22}C_6H_{27}$ .11, C_{16}–$C_2C_1C_3$ .10
140			136	$C_{16}C_2C_1$ .11, $C_{10}C_9N_{22}$ .11
123		122		$C_{20}C_8C_9$ .12
115		110	116	$C_{17}C_3C_2$ .14, H_{27}–$N_{22}C_9C_6$ .10, C_5C_7 .12
84			85	$C_1C_{16}C_2$–$C_3C_{17}C_4$ .10, $C_{17}C_3C_2$ .15
79			85	$C_{12}O_{13}H_{43}$ .13, $C_1C_{16}C_2$–$C_3C_{17}C_4$ .10
67			66	$C_7C_8C_9$–$C_{20}C_{11}H_{37}H_{38}$ .18, $C_6C_{19}C_7$–$C_8C_{20}C_9$ .25
63			64	$C_1O_{15}H_{42}$ .92
49			47	$C_{12}O_{13}H_{43}$ .21, $C_{12}O_{13}H_{44}$ .35
31			31	$H_{31}C_{17}C_3$ .21, $H_{31}C_{17}C_{18}$ .21, $C_3C_{17}C_{18}$ .19

Raman). Eliminating hydrogen bonds changes the composition to vinyl, carbonyl bending and lactam bond stretching at 1161 cm^{-1} on the C–D ring. This band appears as a shoulder on the 1141 cm^{-1} band in vinylisoneoxanthobilirubinate spectra.

The A–B calculation of a pyrrole ring breathing mode at 1187 cm^{-1} is substantiated by the experimental evidence. Bilirubin IXα and all of the model compounds with two pyrromethenone rings have a band at 1188–1192 cm^{-1} in solution Raman spectra. The band is observed at 1185–1186 cm^{-1} in spectra of solid bilirubin IXα and at 1196–1198 cm^{-1} in the half-molecules. The C–D ring calculation predicts this band at 1181 cm^{-1}, a mixture of pyrrole and lactam ring stretches. That there is almost no hydrogen bond sensitivity observed makes this assignment less likely.

The 1200–1300 cm^{-1} region contains several closely spaced and environment-sensitive bands, mostly localized on the lactam moieties. The relative intensities are quite different in resonance Raman and IR spectra. In bilirubin IXα itself the bands are incompletely resolved, and may appear as shoulders or as single broad bands.

The hydrogen-bonded model predicts a lactam-A mode at 1225 cm^{-1} and assigns it to coupled C–C stretches on the lactam ring and vinyl side chain bending. This band can be equated to the 1220 cm^{-1} band in IR spectra. It is very weak in the Raman spectra of hydrogen-bonded molecules. The simplified model predicts no corresponding mode near this region; however, we do observe a shoulder at *ca* 1221 cm^{-1} in Raman spectra of the bilirubin monomer.

The resonance Raman spectra of bilirubin IXα, IIIα and XIIIα all contain at least three bands at *ca* 1250, 1270 and 1285 cm^{-1}. The relative intensities are strongly environment-sensitive and the bands are not always clearly resolved. A propionic acid carbon hydrogen bending mode is calculated (hydrogen-bonded structure) at 1243 cm^{-1}, and may be a component of the strong IR band at 1250 cm^{-1}. However, this vibration cannot contribute to the strong resonance Raman intensity observed near 1250 cm^{-1} in BR IXα and model compounds.

The non-hydrogen-bonded model finds a lactam ring, carbonyl and vinyl group deformation at 1266 cm^{-1} on lactam D and a lactam D stretching mode at 1278 cm^{-1}. These bands are detected in the bilirubin half molecule and bilirubin–lipid complexes as strong and broad bands at *ca* 1268–1276 cm^{-1}. Raman bands at this region are strongly

Table 4. Frequencies and normal coordinate analysis of bilirubin in the range 900–1700 cm^{-1} (CD pyrromethenone)

Calculated	Raman	Coordinates	Assignment
1647		18.3% C_4–C_9, C_{14}–C_{19}, C_{19}–C_{21}, C_9=C_{11}, C_{15}–N_{16}, C_{13}–C_{14}, C_2–C_3	Vinyl coupled lactam and pyrrole ring stretching
1603	1598	34.3% $C_{18}C_{13}C_{14}$, $C_{18}C_{13}C_{12}$, $C_{13}C_{12}N_{16}$, $C_{19}C_{14}C_{13}$ C_{14}=C_{15}, C_{12}–N_{16}	Pyrrole ring deformation
1568	1567	24.4% C_9=C_{11}, C_{21}–C_{22}, C_1–C_2, C_{19}–C_{21}, C_4–C_9, C_{14}–C_{19}, C_{15}–N_{16}, C_5–N_6, C_1–C_{12}, C_3=C_4	Vinyl, lactam C=C, bridge C=C stretching
1552		10.5% N_{16}–H_{17}, C_{14}=C_{15}, C_{21}–C_{22}, C_{12}=C_{13}, C_5=O_{10}, C_2–N_6	Pyrrole C=C, N–H and lactam C=O, C–N stretching
1495	1512	51.8% C_2C_3=C_4C_5, N_6C_2–C_3C_4, C_8–$C_3C_2C_4$, C_9–$C_4C_3C_5$, C_1–$C_2C_3N_6$	Lactam ring torsion
1461	1467	26.7% $C_2C_1C_{12}$, $C_1C_{12}C_{13}$, $C_1C_2C_3$, $C_1C_2N_6$, $C_{12}C_{13}C_{14}$, $C_1C_{12}N_{16}$	Bridge C–C, C=C deformation
1440	1443	74.5% $C_{12}C_{13}$–$C_{14}C_{15}$, $C_{13}C_{14}$=$C_{15}N_{16}$, C_{18}–$C_{13}C_{12}C_{14}$	Pyrrole ring deformation
1427		26.3% $C_{13}C_{14}C_{15}$, $O_{10}C_5C_4$, $C_{20}C_{15}C_{14}$, $C_9C_4C_5$, $C_{19}C_{14}C_{15}$, $C_{19}C_{14}N_{16}$, $C_3C_4C_5$, $C_2C_1C_{12}$	Deformation of C=O and methyl groups on lactam and pyrrole
1329	1337	48.7% C_3C_4–C_5N_6, O_{10}–$C_5C_4N_6$, C_4C_5–N_6C_2, C_9–$C_4C_3C_5$	Lactam torsion
1322	1319	26.3% C_{15}–N_{16}, C_1–C_{12}, C_1–C_2, C_4–C_9, C_{14}–C_{19}, C_5–N_6, C_2–C_3	Pyrrole, lactam ring and bridge stretching
1309		13.7% C_4–C_9, C_{14}–C_{19}, C_9=C_{11}, C_{15}–N_{16}, C_{13}–C_{14}, C_{21}–C_{22}, C_2–C_3, C_5–N_6	Vinyl coupled lactam and pyrrole stretching
1278	1274	18.3% C_{19}–C_{21}, C_4–C_9, C_{21}–C_{22}, C_1–C_{12}, C_9=C_{11}, N_6–H_7, C_1–C_2	Vinyl coupled, bridge C=C, and lactam N–H stretching
1266	1244	24.0% $C_2N_6C_5$, $C_2C_3C_4$, $C_9C_4C_3$, $C_3C_2N_6$, $O_{10}C_5N_6$	Lactam ring and carbonyl deformation

continued on next page

Table 4. *continued*

Calculated	Raman	Coordinates	Assignment
1181	1198	15.9% $C_9{=}C_{11}$, $C_{21}{-}C_{22}$, $C_1{-}C_2$, $C_{19}{-}C_{21}$	Vinyl and bridge C=C stretching
1144	1141	42.4% $C_{22}C_{21}C_{19}$, $C_{21}C_{19}C_{14}$, $C_{18}C_{13}C_{14}$, $C_{20}C_{15}C_{14}$, $C_{21}{-}C_{22}$, $C_{13}{-}C_{18}$	Deformation of methyl group on pyrrole ring
1161		24.1% $C_{11}C_9C_4$, $O_{10}C_5C_4$, $C_8C_3C_4$, $C_5{-}N_6$, $C_2{-}C_3$	Deformation and bond stretching of lactam ring
1107		18.2% $C_9{=}C_{11}$, $C_{21}{-}C_{22}$, $C_1{-}C_2$, $C_{19}{-}C_{21}$, $C_5{-}N_6$, $C_{15}{-}N_{16}$	Vinyl and bridge C=C coupled C–N stretching
1072	1055	10.8% $N_{16}{-}H_{17}$, $C_{14}{=}C_{15}$, $C_{21}{-}C_{22}$, $C_{12}{=}C_{13}$, $C_5{=}O_{10}$, $C_2{-}N_6$	Pyrrole C=C, N–H, lactam C–N and C=O stretching
1032	993	92.15% $N_{16}{-}C_{12}{-}C_1C_2$, $N_6C_2{=}C_1C_{12}$, $C_8{-}C_3C_2C_4$, $C_5N_6{-}C_2C_3$	Bridge C=C and C–C torsion, lactam C–N torsion
945		46.4% $C_{15}{-}C_{20}$, $C_{13}{-}C_{18}$, $C_1{-}C_{12}$, $C_2{-}C_3$, $C_9{=}C_{11}$, $N_6{-}H_7$	Bridge C–C, vinyl, lactam N–H stretch

environmental sensitive. Therefore the assignment to lactum ring modes is realistic; however, neither set of calculations predicts the presence of three bands in this region. While this may be a defect of the models, it is also possible that there is Fermi resonance with the overtone of one of the bands in the 610–640 cm^{-1} region.

The A–B model assigns a bridge C–H bending, bridge C=C stretch, and lactam-A C–N stretch to 1310 cm^{-1}. There are weak bands in the IR (1301 cm^{-1}) and Raman which

Table 5. Comparison of selected bands (cm^{-1}) from the spectra of D_2BR-d^6 and H_2BR in fluorolube

Group	D_2BR-d^6 Calculated	Observed	H_2BR* (in D_2BR)	H_2BR Calculated	Observed
NH pyrrole	2499	2541 2444	3407	3409	3410
NH lactam	2395	2417	3261	3060	3262
CH stretch	3100	3081		3100	3101
CH stretch	3070	3061		3070	3070
CH stretch	3002	3011		3002	3011
C=O C=C	1693	1700		1693	1692
C=O N–C C=O	1655	1640		1655	1649
C=C N–C	1599	1610		1606	1612

* Some H_2BR remains in the spectrum despite the careful sample preparations.

may be this mode. The C–D model predicts a similar vibration at 1309 and 1322 cm^{-1} for pyrrole–lactam ring stretches. These bands are detected at 1319 cm^{-1} as medium-to-strong bands in vinylisoneoxanthobilirubinate aqueous solution.

The C–D model also predicts a lactam ring torsion mode at 1329 cm^{-1}. This may be the weak band at 1337 cm^{-1} in the vinylisoneoxanthobilirubinate spectrum. We have previously observed that in the spectra of bilirubin and its model compounds (BR IIIα, BR XIIIα) this band (at *ca* 1344 cm^{-1}) is sensitive to the vinyl group but insensitive to hydrogen bonding on lactam carbonyl groups. The A–B calculation of methyl C–H bending modes at 1353 and 1356 cm^{-1} may describe the IR spectra adequately, but cannot account for the strong resonance Raman band arising from the A–B ring at *ca* 1344 cm^{-1}. We find it hard to evaluate this assignment conclusively.

The A–B model calculation of a coupled lactam C–N stretch, methyl C–H bending mode at 1395 cm^{-1} fits the observed Raman (1395 cm^{-1}) and IR (1405 cm^{-1}) data well. The C–D model calculation does not contain a similar mode because it does not include the methyl hydrogens.

The non-hydrogen-bonded model calculation shows three bands in the 1427–1460 cm^{-1} region. The pyrrole–C torsion is predicted to be at 1440 cm^{-1}. A C–D pyrrole–lactam bridging carbon deformation is predicted at 1461 cm^{-1}. These two bands correspond to the two hydrogen-bond-sensitive bands at 1443 and 1467 cm^{-1}, respectively, in the Raman spectrum of vinylisoneoxanthobilirubinate.

A vinyl C–H bending mode is calculated (A–B) at 1487 cm^{-1}, and is identified with the 1500 cm^{-1} IR band. The simplified C–D model predicts a lactam D torsional motion at 1495 cm^{-1}. This mode can be equated to the 1512 cm^{-1} band in the vinylisoneoxanthobilirubinate solution spectrum.

The A–B model calculates two bands at 1567 and 1606 cm^{-1}. The IR spectra fit this prediction well. The assignment of a lactam C=C, C–N, C=O, pyrrole C=C stretch is reasonable for the band at *ca* 1605–1616 cm^{-1} observed in bilirubin IXα and other model compounds which have hydrogen bonds. Similarly, the predicted 1567 cm^{-1} backbone stretching mode agrees well with the IR spectra and the solution Raman spectra of acidic forms of bilirubin derivatives. The hydrogen bond sensitivity of this band is consistent with the mode composition.

The C–D model predicts three bands in the 1545–1610 cm^{-1} region. The 1552 cm^{-1} band is weak and not well resolved in the Raman spectrum of vinylisoneoxanthobilirubinate. Bands at 1568 and 1603 cm^{-1} are equated to the weak band at 1567 and a strong band at 1598 cm^{-1}, respectively. The band at 1567 cm^{-1} is calculated to have a similar assignment as in the A–B H-bonded model; however, the 1603 cm^{-1} band is calculated to be a pyrrole-localized vibration. This is characteristic for non-hydrogen-bonded bilirubins. For example, we observe this band at 1597, 1601 and 1598 cm^{-1} in bilirubin IXa/sphingomyelin, bilirubin IIIa/sphingomyelin complex and exovinylneoxatho bilirubinate spectra. This band is obscured by the strong and characteristic 1615 cm^{-1} band of the intramolecularly hydrogen-bonded molecules (BR IIIa, BR IXa, etc.)

Both sets of calculations agree well on the carbonyl stretches at *ca* 1650 cm^{-1}. We have examined the Raman spectra of the α,α'-dimethyl MBR (meso) (Fig. 3) and α,α'-dimethyl MBR (racemic) compounds in chloroform (Fig. 4). The only differences between these two compounds are the orientation of the methyl groups which are in the α position with respect to the carboxylate group. By structural predictions [12] there should be no appreciable differences between the racemic compound and non-substituted MBR XIIIa, while the meso molecule should show steric hindrance from the methyl group, especially in the lactam moiety. In chloroform solvent, where six hydrogen bonds are formed, we observe the band shifting from 1644 to 1648 cm^{-1}. This confirms that the 1644 cm^{-1} band involves largely the lactam ring vibration.

Bands from 2000 to 4000 cm^{-1} have been largely assigned to N–H and C–H stretching. The normal coordinate analysis provides clear answers to some previously posed questions and offers reasonable explanations for the experimental results. For example, in the IR spectrum for the acid salt of calcium bilirubinate (%Ca = 3.2), the relative intensity of the 3410 cm^{-1} bands does change when compared with that of protonated

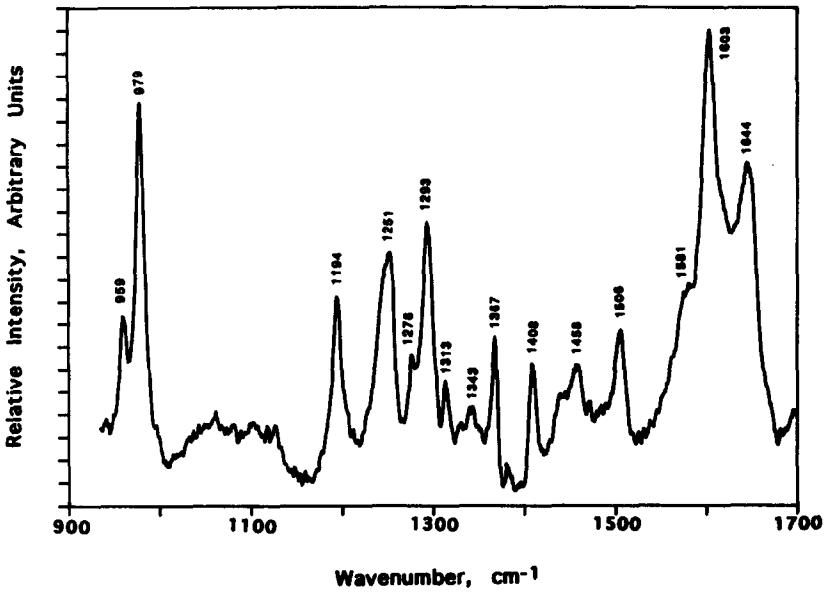

Fig. 3. Resonance Raman spectrum of 5×10^{-4} M α,α'-dimethyl MBR XIIIα (meso) in chloroform; 532 nm excitation.

bilirubin. Thus the 3410 cm^{-1} band cannot be assigned to the OH group. Our calculations indicate that this band is due to the stretching mode of the N–H vibration. The observed result provides evidence that the N–H group coordinates with calcium.

Table 5 shows that in perdeuterated bilirubin, the 3410 cm^{-1} peak of protonated bilirubin, representing the pyrrole N–H, shifts to 2541 cm^{-1}, and the 3260 cm^{-1} peak, assigned as the lactam N–H, shifts to 2444 cm^{-1}. That the peak intensities of the 2541 and 2444 cm^{-1} are more than four times the intensities of the original peaks indicates that most of the N-hydrogens have been replaced by deuterium. Broderson *et al.* [23] obtained similar peak shifts for the pyrrole but not for the lactam bands and found that the peak heights for the shifted bands were about equivalent to the original peaks. He

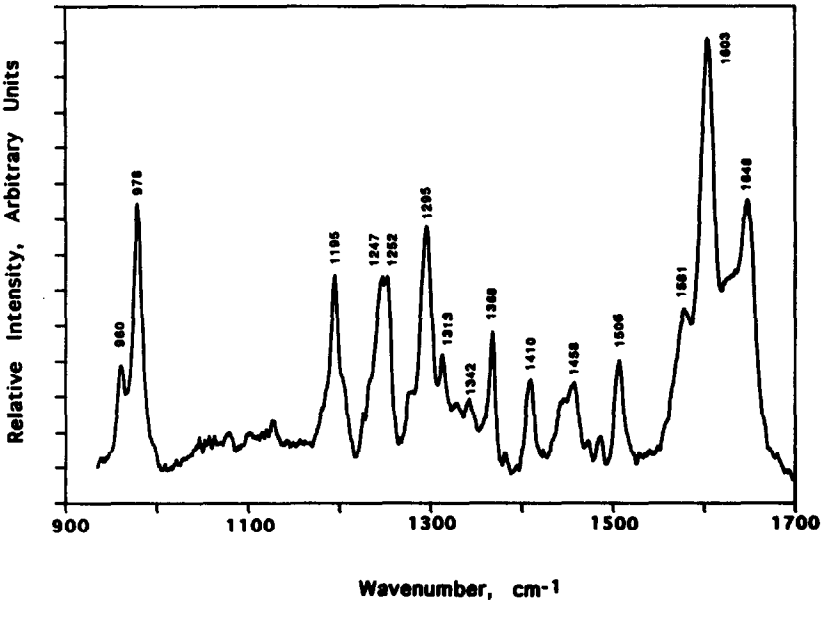

Fig. 4. Resonance Raman spectrum of 5×10^{-4} m α,α'-dimethyl MBR XIIIα (racemic) in chloroform; 532 nm excitation.

concluded that deuterated bilirubin contained only four active hydrogens, two from the carboxyl groups and two from the four nitrogen groups.

Our results, however, indicate that both the pyrrole and lactam groups shift independently as indicated by the relative intensities of the shifted bands. There are several factors which make those band shifts detectable in our experiments. Firstly, our experiments were performed under improved experimental conditions, which permit incorporation of more deuterium. Secondly, we were able to examine the deuterated bilirubin without the need for desiccation. For that we used a fluorolube mull instead of KBr pellets. This process eliminates the trace water in desiccated KBr which undergoes re-exchange with deuterated bilirubin, reducing the proportion of deuteration. In fact, when we made a KBr pellet of D_2BR, we obtained results similar to those of BRODERSON *et al.* [23], in that the 2444 cm^{-1} peak appeared only as a shoulder. Therefore we conclude, and find independent support in the NMR studies of KAPLAN and NAVON [24], that the lactam deuterium may be more active than the pyrrole deuterium, preferentially eliminating this band during pellet formation and explaining why Broderson did not detect the 2444 cm^{-1} band. It is clear that both the previous [23] and present studies support the band assignments proposed in our model.

CONCLUSION

The evaluation of the force field of a molecule as complicated as a bilirubin pyrromethenone is by no means perfect. However, with reasonable molecular models and a realistic potential field, we can make accurate predictions about bilirubins containing or lacking intramolecular hydrogen bonds. Our normal coordinate analysis provides reasonable band assignments for IR Raman bands in the most interesting spectral regions. In addition, the results have clarified a number of obscure or mistaken concepts concerning the spectral and chemical properties of bilirubin.

Acknowledgements—We wish to thank David A. Lightner for providing samples of α,α'-dimethylmesobilirubin (MBR) in the meso and racemic forms. This work was supported in part by NIH grants NS-26160 (to M.D.M.) and AM-16549 (to R.D.S.) and by the State Commission of Education of China (to J.-G.W.).

REFERENCES

[1] J.-G. Wu, R. D. Soloway, D.-F. Xu, X.-Z. Wang, D. K. Martini and A. J. Wagner, *Proc. SPIE* **1145**, 264 (1989).
[2] H. Guo, R. D. Soloway, Z. Yang, X.-C. Ding, D.-F. Xu and J.-G. Wu, *Proc. SPIE* **1145**, 413 (1989).
[3] R. D. Soloway, J.-G. Wu, D.-F. Xu, Y.-F. Zhang, D. K. Martini, N.-K. Hong and R. S. Crowther, *Proc. SPIE* **1145**, 262 (1989).
[4] H. Ishida, R. Kamoto, S. Uchida, A. Ishitani, Y. Ozaki, K. Iriyama, E. Tsukie, K. Shibata, F. Ishihara and H. Kameda, *Appl. Spectrosc.* **41**, 407 (1987).
[5] S. Zheng and A. T. Tu, *Appl. Spectrosc.* **41**, 696 (1987).
[6] Y.-Z. Hsieh and M. D. Morris, *J. Am. Chem. Soc.* **110**, 62 (1988).
[7] B. Yang, M. D. Morris, M. Xie and D. A. Lightner, *Biochemistry* **30**, 688 (1991).
[8] Y.-Z. Hsieh, N.-S. Lee, R.-S. Sheng and M. D. Morris, *Langmuir* **3**, 1441 (1991).
[9] A. F. McDonagh, in *The Porphyrins* (Edited by D. Dolphin), Vol. VI, pp. 293–491. Academic Press, London (1973).
[10] L. Margulies and M. Toporowicz, *J. Molec. Struct.* **174**, 153 (1988).
[11] X.-Z. Wang, R. D. Soloway, J.-G. Wu, B.-Z. Yu and G.-X. Xu, *Proc. SPIE* **1145**, 132 (1989).
[12] G. Puzicha, Y.-M. Pu and D. A. Lightner, *J. Am. Chem. Soc.* **113**, 3583 (1991).
[13] R. Bonnett, J. E. Davies, M. B. Hursthouse and G. M. Sheldrick, *Proc. R. Soc. Lond. (Biol.)* **202**, 249 (1978).
[14] D. P. McDermott, *J. Phys. Chem.* **90**, 2569 (1986).
[15] D. W. Scott, *J. Molec. Spectrosc.* **31**, 451 (1969).
[16] D. W. Scott, *J. Molec. Spectrosc.* **37**, 77 (1971).
[17] P. Császár and A. Császár, *J. Molec. Struct.* **136**, 323 (1986).
[18] G. C. Pimentel and A. L. McClellan, *The Hydrogen Bond.* W. H. Freeman, San Francisco (1960).
[19] E. B. Wilson, J. C. Decius and P. C. Cross, *Molecular Vibrations.* Dover, New York (1955).

[20] C. Califano, *Vibrational States*. John Wiley, London (1976).
[21] J. H. Schatschneider, Reports 231/64 and 57/65, Shell Development Co., West Hollow Research Center, P.O. Box 1380, Houston, Texas (1965).
[22] D. F. McIntosh and M. R. Peterson, *Quantum Chemistry Program Exchange, Program* 342 (1977).
[23] R. Broderson, H. Flodgaard and J. K. Hansen, *Acta. Chem. Scand.* **21**, 2284 (1967).
[24] D. Kaplan and G. Navon, *J. Chem. Soc. Perkin Trans.* **2**, 1374 (1981).